Stochastic Stability of Pile Foundation Systems Under Combined Static, Harmonic and Gaussian White Noise Excitations

Vahdat Samandar Ajirlou and Jian Deng*

Department of Civil Engineering, Lakehead University, Thunder Bay, Ontario, Canada

Abstract: This paper examines the stochastic stability of pile foundations under combined static, harmonic, and random loadings using moment Lyapunov exponents (MLEs) as the primary stability metric. The governing stochastic differential equations are first derived and reduced via stochastic averaging, appropriate for lightly damped systems subjected to weak excitations. Based on the reduced system, a new analytical framework is developed to evaluate MLEs for a pile model, allowing closed-form identification of stability boundaries and critical excitation conditions. Monte Carlo simulation is formulated of the original stochastic system, in which numerical results also provide validation for the analytical predictions from stochastic averaging. As an application, a pile subjected to soil pressure, constant axial load, harmonic excitation, and stochastic disturbances is analyzed. The pile is modeled as a simply supported column resting on a Heténi-type elastic foundation, while the random excitation is represented by Gaussian white noise. The results demonstrate that increases in noise intensity, excitation amplitudes, and load ratios significantly amplify instability, whereas higher damping and foundation stiffness improve stability by reducing MLE values and suppressing higher-mode responses. In addition, longer piles exhibit lower stability, while increased elastic modulus and larger cross-sectional dimensions enhance the overall resistance to instability. The proposed framework provides a rigorous and efficient tool for assessing the stochastic stability of pile systems under complex loading conditions.

Keywords: Stochastic Stability; Moment Lyapunov Exponent; Pile Foundations; Stochastic Averaging; Monte Carlo Simulation.

1. INTRODUCTION

Pile foundations are slender structural members widely employed in civil engineering to support superstructures and transfer loads to deeper, more competent soil strata. One of the principal failure modes of such elements is buckling instability [1,2]. Most previous investigations of pile buckling have primarily considered static loading conditions [3-6]. However, in addition to static axial loads from superstructures, piles may also experience dynamic loads during extreme events such as earthquakes. Several seismic failures of pile-supported structures have been reported, including the collapse of the Showa Bridge during the 1964 Niigata earthquake and the damage to the Harbor Master's Tower at Kandla Port during the 2001 Bhuj earthquake [7]. These observations highlight the importance of investigating the dynamic stability of pile foundations for the safe design and assessment of engineering structures.

Conventional seismic analyses often assume periodic characteristics for seismic waves; however, recorded earthquake motions are inherently aperiodic. This discrepancy necessitates the use of advanced stochastic excitation models capable of representing the irregular nature of seismic inputs and enabling more realistic, empirically based seismic analysis.

Stochastic dynamic analysis is widely applied in civil and mining engineering because many structural loads exhibit inherent randomness. Actions such as earthquakes, turbulent wind, blasting effects, and ocean waves cannot be adequately described by deterministic models and are more appropriately represented using probabilistic descriptions. Consequently, the dynamic behavior of such structures is typically modeled by systems of n-dimensional stochastic differential equations of the following general form.

$$\dot{\mathbf{Z}}(t) = \varepsilon^{\frac{1}{2}}\mathbf{F}\big(\mathbf{Z}, t, \boldsymbol{\xi}(t)\big), \tag{1}$$

where $\mathbf{Z}(t) = \{Z_1, Z_2, \dots, Z_n\}^T$ represents the system state vector and $\boldsymbol{\xi}(t) = \{\xi_1, \xi_2, \dots, \xi_n\}^T$ denotes the vector of stochastic excitations. A fundamental property of stochastic system (1) is its dynamic stability. The sample, or almost sure, stability of the system is characterized by the Lyapunov exponents, which are defined as follows.

$$\lambda_{\mathbf{Z}} = \lim_{t\to\infty}\frac{1}{t}\log\|\mathbf{Z}(t)\|, \tag{2}$$

where $\|\mathbf{Z}(t)\| = \sqrt{\mathbf{Z}^T(t)\mathbf{Z}(t)}$ denotes the Euclidean norm. If the largest Lyapunov exponent is negative, the trivial solution of system (1) is stable with probability one; otherwise, it is almost surely unstable. Lyapunov exponents therefore describe the sample stability or instability of the system. However, almost-sure stability does not necessarily guarantee moment stability. To obtain a comprehensive understanding of the stochastic system's dynamic behavior, both sample stability and moment stability must be examined by

*Address correspondence to this author at the Department of Civil Engineering, Lakehead University, Thunder Bay, Ontario, Canada;
E-mail: jdeng2@lakeheadu.ca

Received on 15-03-2026 Accepted on 05-05-2026 Published on 14-05-2026

E-ISSN: 3083-3590/26

evaluating the Lyapunov exponents as well as the moment Lyapunov exponents (MLEs), since the latter provides information about both moment behavior and almost-sure stability [10].

The stability of the pth moment $\mathrm{E}[\|\mathbf{Z}(t)\|^p]$ of the solution to system (1) is characterized by the pth MLE, defined as follows.

$$\Lambda_{\mathbf{Z}}(p) = \lim_{t\to\infty} \frac{1}{t} \log \mathrm{E}[\|\mathbf{Z}(t)\|^p], \tag{3}$$

where $\mathrm{E}[\cdot]$ denotes the expectation operator. If $\Lambda_{\mathbf{Z}}(p)$ is negative, the pth moment is stable; otherwise, it is unstable. The pth MLE $\Lambda_{\mathbf{Z}}(p)$ is a convex analytic function of p that passes through the origin, and its slope at the origin equals the largest Lyapunov exponent $\lambda_{\mathbf{Z}}$, that is,

$$\lambda_{\mathbf{Z}} = \lim_{p\to 0} \frac{\partial \Lambda_{\mathbf{Z}}(p)}{\partial p}. \tag{4}$$

The nontrivial root $\delta_{\mathbf{Z}}$ of $\Lambda_{\mathbf{Z}}(p)$, satisfying $\Lambda_{\mathbf{Z}}(\delta_{\mathbf{Z}}) = 0$, is referred to as the stability index.

Exact determination of the stability properties (Equation (**2** and **3**)) of stochastic differential system (1) is generally difficult. The stochastic averaging method, originally introduced by Stratonovich [8] and later rigorously established by Khasminskii [9], has been widely applied to obtain approximate solutions for stochastic differential equations containing a small parameter. Under appropriate conditions, stochastic averaging can effectively reduce the dimensionality of system (1), thereby simplifying the analysis [10]. The process $\mathbf{Z}(t)$ can be approximated by an n-dimensional Markov diffusion process $\bar{\mathbf{Z}}(t)$, governed by Equation (**6**), which can also be expressed in the form of Equation (**5**).

$$\mathbf{F} = \mathbf{F}^{(0)}\left(\mathbf{Z}, t, \boldsymbol{\xi}(t)\right) + \varepsilon^{\frac{1}{2}} \mathbf{F}^{(1)}(\mathbf{Z}, t) + o(\varepsilon), \tag{5}$$

$$\mathrm{d}\bar{\mathbf{Z}}(t) = \varepsilon\, \mathbf{m}(\bar{\mathbf{Z}})\mathrm{d}t + \varepsilon^{\frac{1}{2}} \boldsymbol{\sigma}(\bar{\mathbf{Z}})\mathrm{d}\mathbf{W}(t), \tag{6}$$

where $\mathbf{W}(t) = \{W_1, W_2, \dots, W_n\}^T$ denotes an n-dimensional vector of mutually independent standard Wiener processes, and the drift vector $\varepsilon\, \mathbf{m}(\bar{\mathbf{Z}})$ and the $n\times n$ matrix $\varepsilon^{\frac{1}{2}} \boldsymbol{\sigma}(\bar{\mathbf{Z}})$ are given by

$$\begin{cases} \mathbf{m}(\bar{\mathbf{Z}}) = \mathcal{M}_t\left\{\mathbf{F}^{(1)} + \int_{-\infty}^{0} \mathrm{E}\left[\frac{\partial \mathbf{F}^{(0)}}{\partial \mathbf{Z}} \mathbf{F}_{\tau}^{(0)}\right] \mathrm{d}\tau\right\}, \\ \mathbf{b}(\bar{\mathbf{Z}}) = \boldsymbol{\sigma}(\bar{\mathbf{Z}})\boldsymbol{\sigma}^T(\bar{\mathbf{Z}}) = \mathcal{M}_t\left[\int_{-\infty}^{\infty} \mathrm{E}\left[\mathbf{F}^{(0)}\left(\mathbf{F}_{\tau}^{(0)}\right)^T\right] \mathrm{d}\tau\right], \end{cases} \tag{7}$$

$$\mathcal{M}_t(\cdot) = \lim_{T\to\infty} \frac{1}{T} \int_t^{t+T} (\cdot)\, \mathrm{d}t, \tag{8}$$

where $\mathbf{F}_{\tau}^{(0)} = \mathbf{F}^{(0)}(\mathbf{Z}, \boldsymbol{\xi}(t+\tau), t+\tau)$ and $\varepsilon\, \mathbf{b}(\bar{\mathbf{Z}})$ is the $n\times n$ diffusion matrix. $\mathcal{M}_t(\cdot)$ is the averaging operator [10]. The widespread application of stochastic averaging is evidenced by the extensive body of literature on the subject [11-13]. Ariaratnam [14] and Ariaratnam *et al.* [15] applied this technique to analyze viscoelastic systems and coupled linear systems subjected to white-noise excitation. More recently, Hu *et al.* [16] investigated the MLE and stochastic stability characteristics of vibro-impact systems driven by non-Gaussian colored noise. In addition, Deng *et al.* [17,18] employed a combined analytical approach to evaluate the largest Lyapunov exponent and MLE of fractional viscoelastic columns subjected to wideband and bounded noise excitations, while Deng [19] extended the analysis through both theoretical and numerical investigations of coupled viscoelastic systems excited by Ornstein–Uhlenbeck stochastic processes. Furthermore, Namachchivaya and van Roessel [20] examined the MLEs of two coupled elastic oscillators under real noise excitation using stochastic averaging and asymptotic expansion methods. The authors' research team extensively studied the Lyapunov exponent and MLEs of linear elastic systems subjected to single stochastic parametric excitations [21].

Natural hazards pose substantial risks to both human safety and civil infrastructure. Nevertheless, conventional stability analyses frequently evaluate these hazards independently, neglecting potential interaction effects. To address this limitation, the present study investigates the parametric buckling behavior of pile foundations subjected to combined static, harmonic, and stochastic dynamic loading, thereby capturing interaction and amplification mechanisms that are absent in single-hazard assessments.

This study examines the moment stability of a pile foundation system subjected to combined parametric excitations arising from static, harmonic, and stochastic loading. The stochastic averaging method is employed to establish an analytical framework for evaluating the MLEs, and a new procedure is proposed for determining the MLEs of pile foundation systems. Monte Carlo simulation is formulated to provide numerical results and to verify the accuracy of the analytical formulation. The paper is organized as follows: Section 2 presents the governing equations of motion; Section 3 describes the stochastic averaging formulation; Section 4 provides Monte Carlo simulations; Section 5 discusses the results; and Section 6 summarizes the main conclusions. The overall development of the paper is illustrated in Figure **1**.

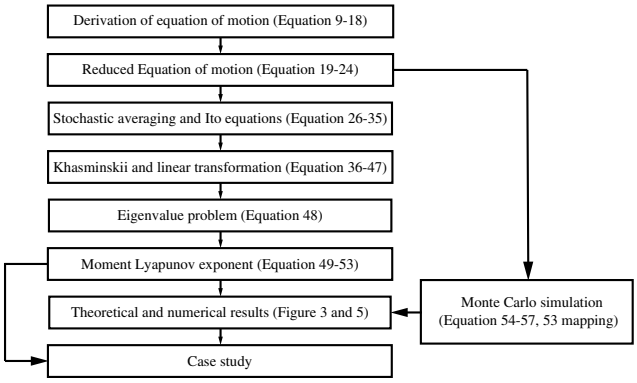

Figure 1: Flowchart of the outline.

2. FORMULATION

To analyze buckling instability, piles embedded in soil, shown in Figure **2**(**a**), can be modeled as beams resting on elastic or viscoelastic foundations [22]. The interaction between structural beams and their supporting soil foundations is fundamentally influenced by foundation type, with early analytical frameworks emerging from 19th-century railroad track studies using elastic foundation beam theory. Over time, diverse mechanical models have been developed to characterize static soil-structure interactions. Despite its limitation in distinguishing between loaded and unloaded zones, the Winkler model has remained widely adopted in dynamic studies due to its computational simplicity [23]. The Winkler model, a foundational one-parameter approach, conceptualizes the foundation as a series of independent linear springs where reaction forces directly correlate with local displacements. To address the Winkler model's limitation in simulating continuum behavior, specifically its inability to account for inter-spring interactions, in this study, the Hetenyi model (integrating flexural rigidity) is employed to represent the soil-pile interaction dynamics, shown in Figure **2(b)**.

To assess pile stability, a thin vertical segment of the pile is analyzed by formulating its governing motion equation, shown in Figure **2(c)**. This equation incorporates the material properties of both the selected segment and the surrounding soil. The derivation employs a force equilibrium approach, where the motion equation is established through force balance principles, a common methodology alongside energy-based equilibrium formulations in such analyses.

The analysis considers a pile of constant cross-section, length L, and flexural stiffness EI. The pile is laterally constrained by surrounding soil, with pinned-pinned boundary conditions at its ends, shown in Figure **2(a)**. The soil-pile interaction is characterized by the subgrade reaction $p(x,\tau)$, which incorporates spring, damper and flexural rigidity effects along the pile length. Dynamic equilibrium accounts for D'Alembert's inertial force $(\rho A \Delta x \ddot{v})$, opposing transverse particle displacement, where ρ denotes mass density, A is the cross-sectional area, and $\ddot{v}$ represents the transverse acceleration. The transverse deformation v, governed by dynamic axial loading, describes the pile's lateral displacement as a function of position x and time τ.

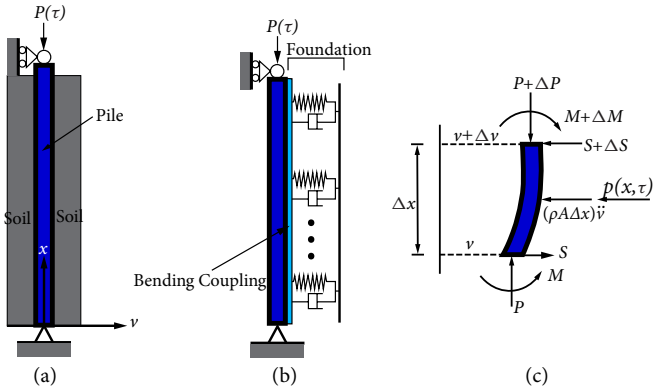

Figure 2: Pile foundation. (a) Soil-embedded pile foundation; (b) Column resting on Hetenyi soil. (c) Free body diagram of the infinitesimal part of pile.

The equilibrium condition for a differential pile segment is defined by enforcing force balance along the vertical axis ($\Delta F = 0$). By resolving horizontal forces in the transverse direction and averaging their vector components, the governing equation for the system is derived.

$$(S + \Delta S) + (\rho A \Delta x)\frac{\partial^2 v(x,\tau)}{\partial \tau^2} - S + p(x,\tau)\times \Delta x = 0,$$

$$\frac{\Delta S}{\Delta x} = -\rho A \frac{\partial^2 v(x,\tau)}{\partial \tau^2} - p(x,\tau). \quad (9)$$

Summing up the moments at the midpoint of the pile segment results in:

$$\Delta M + P(\tau)\Delta v(x,\tau) - S\Delta x + (\rho A \Delta x)\frac{\partial^2 v(x,\tau)}{\partial \tau^2}\frac{\Delta x}{2} + p(x,\tau)\Delta x\frac{\Delta x}{2} = 0, \Delta M + P(\tau)\Delta v(x,\tau) = S\Delta x. \quad (10)$$

Eliminating S from Equation (**9** and **10**) results in:

$$\frac{\partial^2 M}{\partial x^2} = -\rho A \frac{\partial^2 v(x,\tau)}{\partial \tau^2} - p(x,\tau) - P(\tau)\frac{\partial^2 v(x,\tau)}{\partial x^2}, \quad M = EI\frac{\partial^2 v(x,\tau)}{\partial x^2}. \quad (11)$$

The motion equation of the pile can be written as:

$$EI\frac{\partial^4 v(x,\tau)}{\partial x^4} + P(\tau)\frac{\partial^2 v(x,\tau)}{\partial x^2} + \rho A \frac{\partial^2 v(x,\tau)}{\partial \tau^2} + p(x,\tau) = 0. \quad (12)$$

The soil's responsive pressure throughout the length of the pile is determined through taking into

consideration the soil stiffness, damping, and flexural rigidity impact within the soil around the pile [23].

$$p(x,\tau) = k_s v(x,\tau) + c_s \frac{\mathrm{d}v(x,\tau)}{d\tau} + D\frac{\partial^4 v(x,\tau)}{\partial x^4}, \quad (13)$$

where k_s , c_s , and D respectively represent the foundation's stiffness, damping coefficients and bending stiffness per unit length.

Therefore, the governing equation of motion is given by:

$$EI\frac{\partial^4 v(x,\tau)}{\partial x^4} + P(\tau)\frac{\partial^2 v(x,\tau)}{\partial x^2} + \rho A\frac{\partial^2 v(x,\tau)}{\partial \tau^2} + \Big[k_s v(x,\tau) + c_s \frac{\mathrm{d}v(x,\tau)}{d\tau} + D\frac{\partial^4 v(x,\tau)}{\partial x^4}\Big] = 0, \quad (14)$$

where EI represents the flexural stiffness of the pile, ρ denotes the material mass density, and A is the cross-sectional area. The lateral displacement of the pile centerline is expressed as $v(x,\tau)$. The spatial coordinate x is defined along the longitudinal axis of the pile.

To enforce the simply supported boundary conditions, the transverse displacement $v(x,\tau)$ is represented using a Fourier sine series expansion.

$$v(x,\tau) = \sum_{n=1}^{\infty} q_n(\tau)\sin\frac{n\pi x}{L}, n = 1,2,\dots. \quad (15)$$

By substituting Equation (**15**) into Equation (**14**), multiplying the resulting expression by $\sin\left(\frac{n\pi x}{L}\right)$, and integrating over the interval $x \in [0, L]$, the following equation is obtained.

$$\rho A\ddot{q}_n(\tau) + c_s\dot{q}_n(\tau) + \left[k_s + (EI + D)\left(\frac{n\pi}{L}\right)^4 - P(\tau)\left(\frac{n\pi}{L}\right)^2\right]q_n(\tau) = 0. \quad (16)$$

Using a first-mode approximation following Bolotin [26], and assuming small damping and loading amplitudes, the excitation function $P(\tau)$ is taken as the combination of a static component, a harmonic excitation, and a stochastic term, such that $P(\tau) = P_s + P_d\cos(\vartheta_0\tau) + P_r\zeta(\tau)$. Introducing a small parameter $0 < \varepsilon \ll 1$, the resulting governing equation of motion for the pile system can be written as follows.

$$\ddot{q}(\tau) + 2\varepsilon\beta\dot{q}(\tau) + {\Omega_0}^2\left[1 - 2\varepsilon\mu_0\cos\vartheta_0\tau - \gamma_0\varepsilon^{\frac{1}{2}}\zeta(\tau)\right]q(\tau) = 0, \quad (17)$$

$$\begin{cases} P_E = \frac{\pi^2 EI}{L^2}, \lambda = \frac{P_s}{P_E}, \epsilon = \frac{P_d}{P_E}, \kappa = \frac{P_r}{P_E}, \eta = \frac{k_s L^4}{\pi^2 EI}, \omega_0 = \frac{\pi^2}{L^2}\sqrt{\frac{EI}{\rho A}}, \\ {\Omega_0}^2 = {\omega_0}^2\left(1 - \lambda + \eta + \frac{D}{EI}\right), \beta = \frac{c_s}{2\rho A} = \frac{\delta\cdot\Omega_0}{2\pi}, 2\mu_0 = \frac{{\omega_0}^2\epsilon}{{\Omega_0}^2}, \gamma_0 = \frac{{\omega_0}^2\kappa}{{\Omega_0}^2}, \end{cases} \quad (18)$$

where ϑ_0 denotes the circular frequency of the harmonic excitation, and P_E represents the Euler critical buckling load. The parameter λ is the non-dimensional static load, ε corresponds to the non-dimensional dynamic load amplitude, and κ denotes the dimensionless stochastic excitation. The parameter η characterizes the foundation stiffness. The quantity ω_0 is the natural frequency of the pile in free vibration, while Ω_0 represents the natural frequency in the presence of axial loading. The coefficient β describes soil damping, and δ denotes the logarithmic decrement associated with foundation damping [24]. Furthermore, μ_0 and γ_0 are coefficients associated with the harmonic and stochastic loading components, respectively. The parameters P_s, P_d, and P_r represent the amplitudes of the static, harmonic, and stochastic loads, while $\zeta(\tau)$ denotes a Gaussian white stochastic process.

The single-degree-of-freedom (SDOF) formulation in Equation (**17**) is based on the first-mode Galerkin truncation, which is appropriate for slender pile–column systems where instability is primarily governed by the fundamental bending mode. Under parametric excitation, especially near the parametric resonance region, the first mode dominates the dynamic response, and therefore the SDOF approximation provides an accurate and efficient representation of the system. It is acknowledged that higher modes may contribute under conditions such as very long piles or high-frequency excitation.

The soil–structure interaction is represented using a Hetényi-type elastic foundation model, in which bending coupling within the soil is introduced through the fourth-order spatial derivative term $D\frac{\partial^4 v}{\partial x^4}$. This term accounts for flexural interaction between adjacent soil elements and enables the foundation to resist curvature, thereby improving upon the classical Winkler model where soil reactions are independent. In this formulation, the case $D = 0$ reduces to the Winkler model, while nonzero values of D introduce coupling effects similar to those in Pasternak-type foundations. This allows the model to better capture the continuous nature of soil behavior. However, the formulation remains linear and does not include nonlinear soil effects such as yielding, gapping, or degradation under cyclic loading, which represents a limitation of the current approach.

The axial force acting on a pile can be considered as the combination of three distinct components: a static load, a harmonic excitation, and a stochastic disturbance. The static component mainly represents the constant compressive force transmitted from the superstructure and arises primarily from permanent gravity loads, including the weight of structural elements and permanently installed facilities. The

harmonic component accounts for periodic fluctuations in axial force generated by repetitive or cyclic actions, such as rotating machinery, vehicular traffic on bridges, wave loading on offshore structures, or operational loads in wind turbines. In contrast, the stochastic component represents irregular environmental disturbances whose intensity and frequency content vary unpredictably, such as earthquakes, turbulent wind, wave action, and ambient ground vibrations. In practical engineering environments, these loading components typically occur simultaneously. For example, piles supporting bridge structures continuously sustain gravity loads while also being subjected to cyclic traffic-induced forces and occasional random environmental excitations.

Random excitations are commonly modeled using stochastic processes, among which Gaussian white noise represents an important class of wideband random inputs. Gaussian white noise is characterized as a weak stationary process with zero mean and a delta-correlated structure. Mathematically, it can be interpreted as the formal time derivative of a Wiener process and is expressed as $\zeta(\tau) = \sigma_0 \, \mathrm{d}W(\tau)$. This process possesses a constant cosine power spectral density $S(\omega) = \sigma_0^2$ and a sine power spectral density $\Psi(\omega) = 0$ across the entire frequency spectrum. In this formulation, $W(\tau)$ denotes a standard Wiener process, ω represents the natural frequency of the noise, and σ_0 is the diffusion coefficient that defines the intensity of the stochastic excitation.

3. MOMENT LYAPUNOV EXPONENTS USING STOCHASTIC AVERAGING

Equation (**17**) is formulated as a Stratonovich stochastic differential equation (SDE). Determining the moment stability of such systems analytically is generally difficult, since closed-form solutions are rarely available when the stochastic excitation is represented by Brownian motion or Wiener processes. To address this difficulty, the stochastic averaging technique is employed to derive averaged Itô stochastic differential equations governing the evolution of the pth moment [10,25]. The solution of these averaged equations provides the stability conditions, with the moment Lyapunov exponents (MLEs) serving as the stability indicators.

The analysis proceeds as follows. First, the equation of motion in Equation (**17**) is reformulated into an equivalent system of first-order Stratonovich SDEs, presented in Equation (**29**). Next, the stochastic averaging method is applied to transform Equation (**29**) into a set of averaged Itô SDEs, given in Equation (**32**) of Section 3.1. Finally, appropriate stochastic transformations are introduced of Section 3.2 and an associated eigenvalue problem is established to determine the MLEs of Section 3.3.

3.1 Stochastic averaging

To eliminate the damping term in Equation (**17**), the transformation $q(\tau) = x(\tau)\, e^{-\varepsilon\beta\tau}$ is introduced, which leads to the following expression.

$$\ddot{x}(\tau) + {\Omega_0}^2 \left[1 - \frac{\varepsilon^2\beta^2}{{\Omega_0}^2} - 2\varepsilon\mu_0 \cos\vartheta_0\tau - \gamma_0\varepsilon^{\frac{1}{2}}\zeta(\tau)\right] x(\tau) = 0, \tag{19}$$

or

$$\ddot{x}(\tau) + \Omega^2 \left[1 - 2\varepsilon\mu \cos\vartheta_0\tau - \gamma\varepsilon^{\frac{1}{2}}\zeta(\tau)\right] x(\tau) = 0. \tag{20}$$

Applying the time-scaling transformation $t = \Omega\tau$ to Equation (**20**) leads to the following expression.

$$\ddot{x}(t) + \left[1 - 2\varepsilon\mu \cos\vartheta t - \gamma\varepsilon^{\frac{1}{2}}\xi(t)\right] x(t) = 0, \tag{21}$$

$$\xi(t) = \sigma \mathrm{d}W(t), \tag{22}$$

where

$$\Omega^2 = {\Omega_0}^2 - \varepsilon^2\beta^2 \;\;,\;\; \mu = \frac{\mu_0\,{\Omega_0}^2}{{\Omega_0}^2 - \varepsilon^2\beta^2}, \quad \gamma = \frac{\gamma_0\,{\Omega_0}^2}{{\Omega_0}^2 - \varepsilon^2\beta^2} \;,\; \vartheta = \frac{\vartheta_0}{\Omega}, \sigma = \frac{\sigma_0}{\sqrt{\Omega}}. \tag{23}$$

When the stochastic excitation term is removed ($\gamma = 0$), Equation (**21**) reduces to the classical Mathieu Equation

$$\ddot{x}(t) + (1 - 2\varepsilon\mu \cos\vartheta t)x(t) = 0. \tag{24}$$

Parametric resonance of order n occurs when the frequency of the sinusoidal excitation ϑ approaches values close to $\frac{2}{n}$, where $n = 1,2,\ldots$. The primary resonance corresponds to the case $\vartheta \approx 2$, which represents the most critical instability region [26]. Under these conditions, first-order approximations of the instability boundaries can be obtained using either the method of multiple scales or the averaging technique [10].

$$2 - \varepsilon\mu \le \vartheta \le 2 + \varepsilon\mu. \tag{25}$$

To obtain a first-order approximation of the instability region of Equation (**21**) using the stochastic averaging method, the following coordinate transformation is introduced:

$$x(t) = a_1(t)\cos(t) + a_2(t)\sin(t)\,, \dot{x}(t) = -a_1(t)\sin(t) + a_2(t)\cos(t). \tag{26}$$

By differentiating the first expression in Equation (**26**) and equating it with the second expression, the following relation is obtained:

$$\dot{a}_1(t)\cos(t) + \dot{a}_2(t)\sin(t) = 0. \tag{27}$$

By differentiating the second expression in Equation (**26**) and substituting the resulting relation into Equation (**21**), and then combining it with the original expressions in Equation (**26**), the following system is obtained:

$$-\dot{a}_1(t)\sin(t) + \dot{a}_2(t)\cos(t) = \varepsilon[a_1(t)\cos(t) + a_2(t)\sin(t)] + \varepsilon^{\frac{1}{2}}\gamma\xi(t)[a_1(t)\cos(t) + a_2(t)\sin(t)]. \tag{28}$$

Solving Equation (**27** and **28**) for the case of primary resonance, with $\vartheta = 2$, results in the following equation of motion.

$$\begin{bmatrix}\dot{a}_1(t)\\ \dot{a}_2(t)\end{bmatrix} = \varepsilon\mathcal{F}^{(1)}(a_1, a_2, t) + \varepsilon^{\frac{1}{2}}\mathcal{F}^{(0)}(a_1, a_2, \xi, t). \tag{29}$$

Here, $\mathcal{F}^{(1)}(a_1, a_2, t)$ represents the drift term, while $\mathcal{F}^{(0)}(a_1, a_2, \xi, t)$ corresponds to the diffusion term.

$$\mathcal{F}^{(1)}(a_1, a_2, t) = \begin{bmatrix}\mathcal{F}_1^{(1)}(a_1,a_2,t)\\ \mathcal{F}_2^{(1)}(a_1,a_2,t)\end{bmatrix} = \begin{Bmatrix}2\mu\cos\vartheta t\left[\frac{-a_1(t)}{2}\sin(2t) - a_2(t)\sin^2 t\right]\\ 2\mu\cos\vartheta t\left[a_1(t)\cos^2 t + \frac{a_2(t)}{2}\sin(2t)\right]\end{Bmatrix}, \tag{30}$$

$$\mathcal{F}^{(0)}(a_1, a_2, \xi, t) = \begin{bmatrix}\mathcal{F}_1^{(0)}(a_1,a_2,\xi,t)\\ \mathcal{F}_2^{(0)}(a_1,a_2,\xi,t)\end{bmatrix} = \begin{Bmatrix}-\gamma\xi(t)\left[\frac{a_1(t)}{2}\sin(2t) + a_2(t)\sin^2 t\right]\\ \gamma\xi(t)\left[a_1(t)\cos^2 t + \frac{a_2(t)}{2}\sin(2t)\right]\end{Bmatrix}. \tag{31}$$

The transformation to amplitude–phase variables is based on separating the response into fast oscillatory components and slowly varying amplitudes. The variables $a_1(t)$ and $a_2(t)$ evolve on a slow time scale due to the presence of the small parameter, while the trigonometric terms represent fast oscillations. By substituting this transformation into the governing equation and enforcing consistency conditions, a system of SDEs describing the slow dynamics is obtained.

An exact analytical solution of Equation (**29**) is generally difficult to obtain because of the complexity of the system. However, the presence of the small parameter ε ensures that the terms on the right-hand side remain of small magnitude. As a result, the variables a_1 and a_2 vary slowly with time. This property allows the system response to be averaged over one excitation period T, providing sufficiently accurate approximations. The averaging procedure can be carried out using the operator in Equation (**8**). The averaging operator performs integration with respect to the explicit time variable t appearing in the integrand. By applying the stochastic averaging procedure, Equation (**29**) can be approximated by a set of Itô SDEs:

$$\mathrm{d}\begin{pmatrix}\bar{a}_1\\ \bar{a}_2\end{pmatrix} = \varepsilon\begin{pmatrix}\overline{m}_{a_1}\\ \overline{m}_{a_2}\end{pmatrix}\mathrm{dt} + \varepsilon^{\frac{1}{2}}\begin{bmatrix}\overline{\sigma}_{11} & \overline{\sigma}_{12}\\ \overline{\sigma}_{21} & \overline{\sigma}_{22}\end{bmatrix}\begin{bmatrix}\mathrm{d}W_1\\ \mathrm{d}W_2\end{bmatrix}. \tag{32}$$

Here, $W_i(t), i = 1{,}2,$ denotes standard Wiener processes. During the averaging procedure, $\bar{a}_1(t)$ and $\bar{a}_2(t)$ are treated as slowly varying quantities and are therefore approximated as constants, denoted simply by $\bar{a}_1$ and $\bar{a}_2$. With this approximation, the following expression is obtained:

$$\begin{cases}\overline{m}_{a_1} = \frac{1}{8}\gamma^2[\mathcal{S}(2) - \mathcal{S}(0)]\bar{a}_1 + \frac{1}{2}\mu\bar{a}_2,\\ \overline{m}_{a_2} = \frac{1}{2}\mu\bar{a}_1 + \frac{1}{8}\gamma^2[\mathcal{S}(2) - \mathcal{S}(0)]\bar{a}_2,\end{cases} \tag{33}$$

$$\begin{cases}[\bar{\sigma}\bar{\sigma}^T]_{11} = b_{11} = \frac{1}{8}\gamma^2[\mathcal{S}(2) + 2\mathcal{S}(0)]{\bar{a}_2}^2 + \frac{1}{8}\gamma^2\mathcal{S}(2){\bar{a}_1}^2,\\ [\bar{\sigma}\bar{\sigma}^T]_{12} = b_{12} = [\bar{\sigma}\bar{\sigma}^T]_{21} = b_{21} = -\frac{1}{4}\gamma^2\bar{a}_1\bar{a}_2\mathcal{S}(0),\\ [\bar{\sigma}\bar{\sigma}^T]_{22} = b_{22} = \frac{1}{8}\gamma^2[\mathcal{S}(2) + 2\mathcal{S}(0)]{\bar{a}_1}^2 + \frac{1}{8}\gamma^2\mathcal{S}(2){\bar{a}_2}^2.\end{cases} \tag{34}$$

The cosine power spectral density function of the noise process $\xi(t)$ is given by:

$$\begin{cases}\mathcal{S}(2) = \int_{-\infty}^{+\infty}\mathcal{R}(\tau)\cos(2\tau)\,\mathrm{d}\tau = 2\int_0^{+\infty}\mathcal{R}(\tau)\cos(2\tau)\,\mathrm{d}\tau = 2\int_{-\infty}^{0}\mathcal{R}(\tau)\cos(2\tau)\,\mathrm{d}\tau,\\ \mathcal{S}(0) = \int_{-\infty}^{+\infty}\mathcal{R}(\tau)\,\mathrm{d}\tau = 2\int_0^{+\infty}\mathcal{R}(\tau)\,\mathrm{d}\tau = 2\int_{-\infty}^{0}\mathcal{R}(\tau)\,\mathrm{d}\tau,\end{cases} \tag{35}$$

where $R(\tau) = E[\xi(t)\xi(t+\tau)]$ denotes the autocorrelation function of the stochastic process $\xi(t)$. For a white noise process, the cosine power spectral density is constant over all frequencies, and therefore $\mathcal{S}(2) = \mathcal{S}(0) = \sigma^2$.

The averaging process constructs an equivalent reduced-order Markov diffusion process whose statistical properties approximate those of the original system over long-time intervals. This is achieved by applying the averaging operator, defined as a time average over the fast variable, to the drift and diffusion terms of the Stratonovich SDEs. In particular, the drift term of the averaged system consists of two contributions: the direct average of the deterministic perturbation terms and an additional correction term arising from the interaction between the stochastic excitation and the system dynamics, expressed through correlation integrals. Similarly, the diffusion coefficients are obtained from the autocorrelation structure of the stochastic excitation, ensuring that the second-order statistics of the original system are preserved.

This procedure leads to an Itô stochastic differential equation governing the evolution of the slow variables. The transition from the Stratonovich to the Itô

formulation is essential, as it ensures that the resulting system satisfies the Markov property and allows the use of Itô calculus for further analysis. The averaged system captures the long-term statistical behavior of the original dynamics, including the effects of noise intensity and spectral characteristics, rather than merely filtering out oscillatory components.

3.2 Mathematical transformation

The MLEs can be obtained from Equation (**32**) by applying the transformation introduced by Khasminskii [9] to the Itô SDEs describing the amplitude evolution.

$$r = \sqrt{\bar{a}_1{}^2 + \bar{a}_2{}^2}, \theta = \tan^{-1}\frac{\bar{a}_2}{\bar{a}_1}, \bar{a}_1 = r\cos\theta\,, \bar{a}_2 = r\sin\theta\,, P = r^p. \tag{36}$$

Consequently, the MLE is expressed as:

$$\Lambda(p) = \lim_{t\to\infty}\frac{1}{t}\log \mathrm{E}[P]. \tag{37}$$

The Itô SDEs describing the evolution of the variable P are obtained by applying Itô's lemma [10]:

$$\mathrm{d}P = m_P(P,\theta)\mathrm{d}t + \sigma_P \mathrm{d}W(t) = m_P(P,\theta)\mathrm{d}t + \sigma_{P1}\mathrm{d}W_1 + \sigma_{P2}\mathrm{d}W_2, \tag{38}$$

where

$$\begin{cases} m_P(P,\theta) = \frac{\varepsilon p P}{16}[8\mu\sin(2\theta) + \sigma^2\gamma^2(p+2)], \\ \sigma_P{}^2 = \sigma_{P1}{}^2 + \sigma_{P2}{}^2 = \frac{\varepsilon p^2 P^2}{8}\sigma^2\gamma^2. \end{cases} \tag{39}$$

Hence,

$$\mathrm{d}\theta = m_\theta(\theta)\mathrm{d}t + \sigma_\theta \mathrm{d}W(t) = m_\theta(\theta)\mathrm{d}t + \sigma_{\theta1}\mathrm{d}W_1 + \sigma_{\theta2}\mathrm{d}W_2, \tag{40}$$

where

$$\begin{cases} m_\theta(\theta) = \frac{\varepsilon\mu}{2}\cos(2\theta)\,, \\ \sigma_\theta{}^2 = \sigma_{\theta1}{}^2 + \sigma_{\theta2}{}^2 = \frac{3}{8}\varepsilon\sigma^2\gamma^2. \end{cases} \tag{41}$$

The coefficients in the amplitude equation (Equation (**33**)), such as $\overline{m}_{a_i}$ for $i = 1,2$, are homogeneous of degree one with respect to $\bar{a}_1$ and $\bar{a}_2$. Consequently, the associated diffusion term $\boldsymbol{b}$ becomes homogeneous of degree two in these variables. Introducing the polar coordinate transformation $\bar{a}_1 = r\cos\theta$ and $\bar{a}_2 = r\sin\theta$ from Equation (**36**) into Equation (**38**) shows that the drift term $m_P(P,\theta)$ and the diffusion terms σ_{P1} and σ_{P2} depend on both P (with degree-one homogeneity) and θ. In contrast, the drift $m_\theta(\theta)$ and diffusion coefficient $\sigma_{\theta1}$ and $\sigma_{\theta2}$ in Equation (**40**) depend only on θ. This indicates that the processes $P(t)$ in Equation (**38**) and $\theta(t)$ in Equation (**40**) remain coupled, even though $\theta(t)$ itself evolves as an autonomous diffusion process.

To determine the MLE, a linear stochastic transformation is introduced.

$$S = \mathcal{T}(\theta)P, P = \mathcal{T}(\theta)^{-1}S, 0 \le \theta < \pi. \tag{42}$$

The Itô SDE describing the transformed P-th norm process S is obtained through the application of Itô's lemma.

$$\mathrm{d}S = m_S\mathrm{d}t + \left(\sigma_{P1}\frac{\partial S}{\partial P}\mathrm{d}W_1 + \sigma_{P2}\frac{\partial S}{\partial P}\mathrm{d}W_2 + \sigma_{\theta1}\frac{\partial S}{\partial\theta}\mathrm{d}W_1 + \sigma_{\theta2}\frac{\partial S}{\partial\theta}\mathrm{d}W_2\right). \tag{43}$$

The drift coefficient can be obtained by

$$m_S = m_P\frac{\partial S}{\partial P} + m_\theta\frac{\partial S}{\partial P} + \frac{1}{2}\left[b_{11}^S\frac{\partial^2 S}{\partial P^2} + (b_{12}^S + b_{21}^S)\frac{\partial^2 S}{\partial P\partial\theta} + b_{22}^S\frac{\partial^2 S}{\partial\theta^2}\right], \tag{44}$$

and the relation for the diffusion terms is given by

$$b^S = \left[\sigma^S\sigma^{S^T}\right], \sigma^S = \begin{bmatrix}\sigma_{P1} & \sigma_{P2}\\ \sigma_{\theta1} & \sigma_{\theta2}\end{bmatrix}. \tag{45}$$

Substituting σ_{P1} and σ_{P2} from Equation (**38**) and $\sigma_{\theta1}$ and $\sigma_{\theta2}$ from Equation (**40**) into Equation (**45**) lead to

$$b_{11}^S = \sigma_P{}^2,\ b_{22}^S = \sigma_\theta{}^2, b_{12}^S = b_{21}^S = 0. \tag{46}$$

If the transformation $T(\theta)$ is bounded and nonsingular, the stability behavior of the processes P and S remains unchanged. Therefore, the transformation $T(\theta)$ is constructed so that the drift component in the Itô differential equation (Equation **43**) no longer depends on the phase variable θ.

$$\mathrm{d}S = \Lambda S\mathrm{d}t + \varepsilon^{\frac{1}{2}}(\sigma_{S1}\mathrm{d}W_1 + \sigma_{S2}\mathrm{d}W_2). \tag{47}$$

By comparing the drift components of Equation (**43** and **47**), the appropriate form of the transformation $\mathcal{T}(\theta)$ can be determined as follows,

$$\frac{1}{16}[p(p+2)\sigma^2\gamma^2\mathcal{T}_\theta + 3\sigma^2\gamma^2\mathcal{T}_\theta'' + 8p\mu\sin(2\theta)\mathcal{T}_\theta + 8\mu\cos(2\theta)\,\mathcal{T}_\theta'] = \hat{\Lambda}\mathcal{T}_\theta, 0 \le \theta < \pi. \tag{48}$$

In this formulation, $\mathcal{T}(\theta)$ is a π-periodic function of θ. Equation (**48**) therefore defines an eigenvalue problem associated with a second-order differential operator, where Λ denotes the eigenvalue and $\mathcal{T}(\theta)$ is the corresponding eigenfunction.

Taking the expectation of both sides of Equation (**47**) and using the property $E[\sigma_{S1}dW_1 + \sigma_{S2}dW_2] = 0$, the relation $dE[S] = \Lambda E[S]dt$ is obtained. This result shows that Λ corresponds to the Lyapunov exponent that governs the stability of the pth moment of the system described by Equation (**21**). Since the transformation between P and S is bounded and nonsingular, both processes exhibit identical stability characteristics.

To determine the MLEs, the amplitude variables are transformed into polar coordinates, where the radial component represents the response magnitude and the angular component represents the phase. The SDE governing the radial process is then used to define the evolution of the p-th moment.

3.3 Moment Lyapunov exponents

Since the coefficients in Equation (**48**) are periodic with period π, the eigenfunction $T(\theta)$ can be effectively represented using a Fourier series expansion.

$$\mathcal{T}(\theta) = \mathcal{C}_0 + \sum_{k=1}^{K}(\mathcal{C}_k \cos 2k\theta + \mathcal{D}_k \sin 2k\theta). \quad (49)$$

Equation (**49**) is substituted into Equation (**48**), and then the terms with the same trigonometric functions $\cos 2k\theta$ and $\sin 2k\theta$ for $k = 0, 1, 2 \ldots K$, are grouped together. By setting the coefficients of these terms equal, a system of homogeneous linear equations is obtained for the unknown coefficients $\mathcal{C}_0$, $\mathcal{C}_k$ and $\mathcal{D}_k$, $k = 1, 2 \ldots K$.

$$\begin{bmatrix} a_{00}^{\mathcal{C}} - \hat{\Lambda}_{x(t)}^{(K)} & a_{01}^{\mathcal{C}} & a_{01}^{\mathcal{D}} & a_{02}^{\mathcal{C}} & a_{02}^{\mathcal{D}} & \cdots \\ a_{10}^{\mathcal{C}} & a_{11}^{\mathcal{C}} - \hat{\Lambda}_{x(t)}^{(K)} & a_{11}^{\mathcal{D}} & a_{12}^{\mathcal{C}} & a_{12}^{\mathcal{D}} & \cdots \\ b_{10}^{\mathcal{C}} & b_{11}^{\mathcal{C}} & b_{11}^{\mathcal{D}} - \hat{\Lambda}_{x(t)}^{(K)} & b_{12}^{\mathcal{C}} & b_{12}^{\mathcal{D}} & \cdots \\ a_{20}^{\mathcal{C}} & a_{21}^{\mathcal{C}} & a_{21}^{\mathcal{D}} & a_{22}^{\mathcal{C}} - \hat{\Lambda}_{x(t)}^{(K)} & a_{22}^{\mathcal{D}} & \cdots \\ b_{20}^{\mathcal{C}} & b_{21}^{\mathcal{C}} & b_{21}^{\mathcal{D}} & b_{22}^{\mathcal{C}} & b_{22}^{\mathcal{D}} - \hat{\Lambda}_{x(t)}^{(K)} & \ddots \\ \vdots & \vdots & \vdots & \vdots & \vdots & \end{bmatrix} \begin{bmatrix} \mathcal{C}_0 \\ \mathcal{C}_1 \\ \mathcal{D}_1 \\ \mathcal{C}_2 \\ \mathcal{D}_2 \\ \vdots \end{bmatrix} = 0. \quad (50)$$

For the coefficients $\mathcal{C}_0$, $\mathcal{C}_k$ and $\mathcal{D}_k$, to have a non-zero (non-trivial) solution, the determinant of the corresponding coefficient matrix must be equal to zero. This requirement leads to a polynomial equation of order $2K + 1$, from which the approximate eigenvalue $\hat{\Lambda}_{x(t)}^{(K)}$ can be determined.

$$e_{2K+1}^{(K)}\left[\hat{\Lambda}_{x(t)}^{(K)}\right]^{2K+1} + e_{2K}^{(K)}\left[\hat{\Lambda}_{x(t)}^{(K)}\right]^{2K} + \cdots + e_1^{(K)}\hat{\Lambda}_{x(t)}^{(K)} + e_0^{(K)} = 0, \quad (51)$$

where $\hat{\Lambda}_{x(t)}^{(K)}$ represents the approximate moment Lyapunov exponent obtained by truncating the Fourier series expansion of the eigenfunction $\mathcal{T}(\varphi)$ up to order K. Accordingly, the moment Lyapunov exponent of the system described in Equation (**21**) can be approximated as follows:

$$\Lambda_{x(t)}^{(K)} \approx \varepsilon\hat{\Lambda}_{x(t)}^{(K)}. \quad (52)$$

A relationship can be established between the moment Lyapunov exponents of the dynamical systems governed by Equation (**17** and **21**), which is given by the following expression:

$$\Lambda_{q(\tau)}^{(K)}(p) = -\varepsilon p\beta + \Lambda_{x(\tau)}^{(K)}(p) = -\varepsilon p\beta + \Omega\Lambda_{x(t)}^{(K)}(p). \quad (53)$$

4. MONTE CARLO SIMULATION

Monte Carlo simulation is employed to evaluate the pth MLEs numerically and to assess the accuracy of the approximate solutions obtained through stochastic averaging. Assume that the excitation is modeled as Gaussian white noise with a constant spectral density $S(\omega) = \sigma^2$ for all the frequency ω. Under this assumption, $\xi(t)\,\mathrm{d}t = \sigma\,\mathrm{d}W(t)$, with the core procedure defined as follows,

$$x_1(t) = x(t),\ x_2(t) = \dot{x}(t). \quad (54)$$

Equation (**21**) can be rewritten in the form of a two-dimensional dynamical system,

$$\begin{cases} \dot{x}_1(t) = x_2, \\ \dot{x}_2(t) = \left(-1 + 2\varepsilon\mu\cos\vartheta t + \gamma\varepsilon^{\frac{1}{2}}\xi(t)\right)x_1. \end{cases} \quad (55)$$

Equation (**55**) can be discretized using the explicit Taylor scheme

$$\begin{cases} {x_1}^{\varkappa+1} = {x_1}^{\varkappa} + {x_2}^{\varkappa}\cdot\Delta t + 0.5R^{\varkappa}\cdot(\Delta t)^2, \\ {x_2}^{\varkappa+1} = {x_2}^{\varkappa} + R^{\varkappa}\cdot\Delta t + 0.5[(-1 + 2\varepsilon\mu\cos\vartheta t){x_2}^{\varkappa}]\cdot(\Delta t)^2 + \sigma\gamma\varepsilon^{\frac{1}{2}}{x_1}^{\varkappa}\cdot\Delta W^{\varkappa} \\ \quad +0.5\sigma\gamma\varepsilon^{\frac{1}{2}}{x_2}^{\varkappa}\cdot\Delta t\cdot\Delta W^{\varkappa}, R^{\varkappa} = (-1 + 2\varepsilon\mu\cos\vartheta t){x_1}^{\varkappa}, \end{cases} \quad (56)$$

where Δt is the time step size, and the superscript $\varkappa$ denotes that the quantity is evaluated at time $t_{\varkappa}$. Following discretization, a time series of the response variable $x(t)$ is generated for specified initial conditions.

The Taylor scheme is used in simulations to estimate statistical measures, such as MLEs, rather than to track exact sample paths. Therefore, weak convergence is sufficient, as the goal is to accurately capture expected values. For the linear stochastic system considered, the weak Taylor scheme provides reliable accuracy. Although strong excitation may reduce the accuracy of stochastic averaging due to its underlying assumptions, Monte Carlo simulations of the original system remain valid when a sufficiently small-time step is used. To ensure accuracy, the time step is selected to be much smaller than the system's natural period and is further refined until consistent results are obtained.

Using $\mathbb{S}$ independent sample paths obtained from the stochastic differential equations, the pth moment of the response is estimated as

$$\mathrm{E}[\|\mathbf{x}(t_{\varkappa})\|^p] = \frac{1}{\mathbb{S}}\sum_{\mathfrak{s}=1}^{\mathbb{S}}\|\mathbf{x}^{\mathfrak{s}}(t_{\varkappa})\|^p,\ \|\mathbf{x}^{\mathfrak{s}}(t_{\varkappa})\| = \sqrt{\left(\mathbf{x}^{\mathfrak{s}}(t_{\varkappa})\right)^T\mathbf{x}^{\mathfrak{s}}(t_{\varkappa})}. \quad (57)$$

where $\mathbf{x}^{\mathfrak{s}}(t_{\varkappa})$ denotes the $\mathfrak{s}$ th realization of the response vector at time $t_{\varkappa}$, and $\|\mathbf{x}^{\mathfrak{s}}(t_{\varkappa})\|$ is its Euclidean norm.

5. RESULTS AND DISCUSSION

A simply supported pile with a solid circular cross-section is considered subjected to combined

static, dynamic, stochastic axial loads. The cylindrical structure has a diameter of D =600 mm, and total length $L = 45$ m. Its cross-sectional area A is calculated as $0.28\ \mathrm{m}^2$ with material density $\rho = 7.8\times10^3\mathrm{kg/m}^3$ and Young's elastic modulus $E = 3\times10^4$ MPa. The moment of inertia for tubular cross-section's is $6.36\times10^{-3}\mathrm{m}^4$ [27].

$$I = \pi\times\frac{(0.6)^4}{64} = 6.36\times10^{-3}\ \mathrm{m}^4. \tag{58}$$

The Euler buckling load, the pile's natural frequency and modified one, and the damping of the system are (see Equation (**18**))

$$P_E = EI\left(\frac{\pi}{L}\right)^2 = 3\times10^{10}\times6.36\times10^{-3}\times\left(\frac{\pi}{45}\right)^2 = 0.93\ \mathrm{MN}, \tag{59}$$

$$\omega_0 = \left(\frac{\pi}{L}\right)^2\sqrt{\frac{EI}{\rho A}} = \left(\frac{\pi}{45}\right)^2\sqrt{\frac{3\times10^4\times6.36\times10^{-3}}{7.8\times10^3\times0.28}} = 1.44\ \frac{\mathrm{rad}}{\mathrm{s}} = 0.22\ \mathrm{Hz}, \tag{60}$$

$$\Omega_0{}^2 = \omega_0{}^2(1-\lambda+\eta) = 1.43^2\times\left(1-\lambda+\eta+\frac{D}{EI}\right) = 2.05\times\left(1-\lambda+\eta+\frac{D}{EI}\right), \tag{61}$$

$$\beta = \frac{\delta\cdot\Omega}{2\pi} = 0.22\times\delta\times\sqrt{1-\lambda+\eta+\frac{D}{EI}}, \tag{62}$$

$$\Omega^2 = \Omega_0{}^2 - \varepsilon^2\beta^2 = \left(1-\lambda+\eta+\frac{D}{EI}\right)(2.05-0.05\varepsilon^2\delta^2). \tag{63}$$

Then the natural period is $\mathfrak{T}_0 = \frac{2\pi}{\omega_0} = 4.38$ s. The effect of critical parameters on stochastic stability and parametric resonance phenomena of the pile foundation is studied, with theoretical insights rigorously validated through numerical simulations.

5.1. Effect of stochastic excitation

Figure (**3** and **4**) indicate that increasing the noise intensity σ leads to a stronger parametric resonance response, as reflected by the growth in the absolute values of the MLEs for σ_0= 0.49, 0.98, 1.47, and 1.96. The analytical predictions are in close agreement with the Monte Carlo results presented in Figure **3**, where the simulations are carried out using a sample size of $\mathbb{S}$ = 300, M = 200-time segments, $\mathcal{K}$ = 500 iterations per segment, a time increment of Δt = 0.005, and a total simulation duration of $\mathbb{T}$ = 500.

For the case of $\sigma = 1$, the comparison between the analytical and numerical moment Lyapunov exponents demonstrates a generally consistent trend across the entire range of p. The maximum absolute error is found to be approximately 0.0231, occurring at the extreme value $p = 4$. This indicates that the discrepancy between the analytical solution obtained via stochastic averaging and the numerical results from Monte Carlo simulation remains relatively small in magnitude. The agreement is particularly strong near the central region around $p = 0$, while deviations increase gradually toward larger values of $|p|$. Overall, these results confirm that the analytical approach provides a reasonably accurate approximation of the system behavior for $\sigma = 1$, with bounded error even at higher-order moments.

A convergence study was also performed with respect to the time step Δt and number of sample paths $\mathbb{S}$. It was observed that reducing Δt below 0.005 and increasing $\mathbb{S}$ beyond 300 resulted in negligible changes in the estimated MLEs, indicating numerical convergence of the Monte Carlo simulations.

The truncation order K in the Fourier expansion (Equation (**49**)) controls the accuracy of the eigenvalue approximation. In this study, values of $K \geq 4$ were found to provide a good balance between computational efficiency and accuracy. A sensitivity analysis was conducted by increasing K, and it was observed that the variation in the computed MLEs becomes negligible for $K \geq 4$, indicating convergence of the solution. Therefore, the selected truncation orders ensure reliable approximation of the eigenvalue problem.

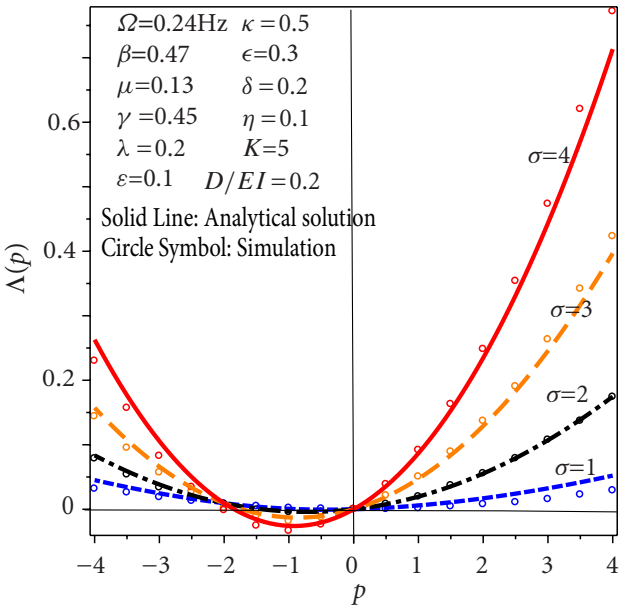

Figure 3: Impact of noise intensity σ on MLEs.

Figure **5** shows that increasing the excitation amplitude γ in Equation (**23**) amplifies the magnitude of the MLEs for κ= 0.9, 1.8, 2.7, and 3.6, indicating a stronger parametric resonance response; this trend is also evident in the three-dimensional representation in Figure **6**. Moreover, the close agreement between the Monte Carlo simulations and the analytical predictions obtained from the numerical procedure in Figure (**3** and

5) confirm the validity and accuracy of the proposed theoretical framework.

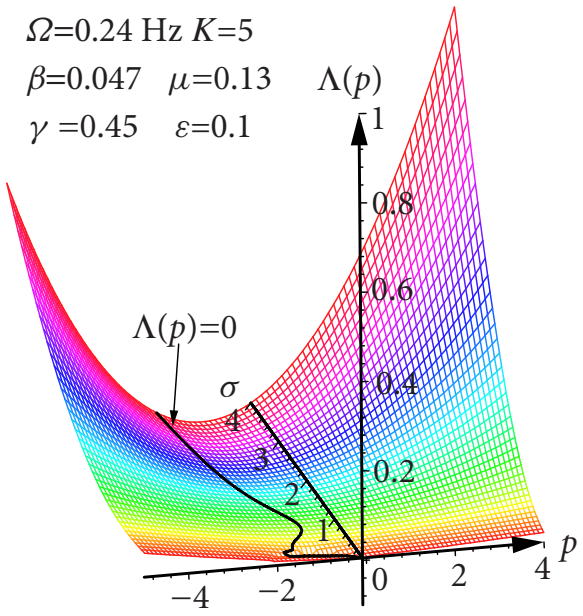

Figure 4: Three-dimensional MLE for noise intensity σ.

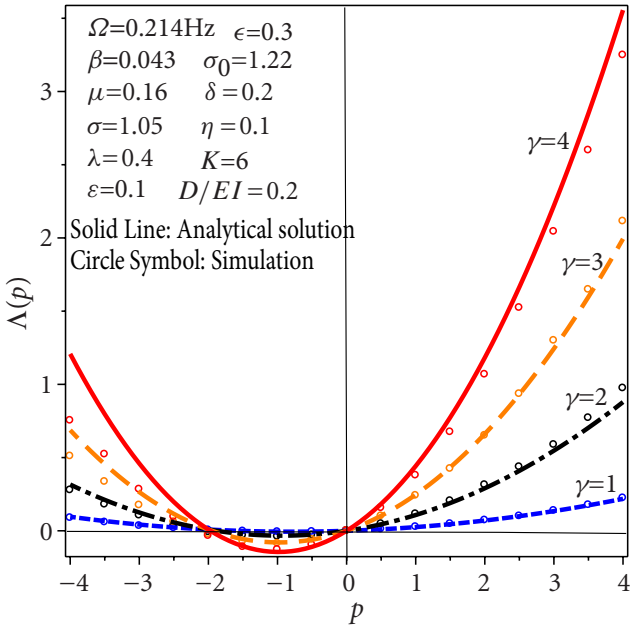

Figure 5: Influence of amplitude of noise γ on MLEs.

5.2. Effect of Deterministic Excitation

Figure **7** highlights the critical role of the harmonic excitation amplitude μ in governing system stability, showing that larger values of μ produce higher MLEs and consequently intensify instability. The figure also presents the response under different dynamic load amplitudes (ϵ = 0.1, 0.3, 0.5, 0.7), where increasing ϵ progressively shrinks the stable domain for $p > 0$. This destabilizing influence of μ is further visualized in the three-dimensional representation in Figure **8**. In addition, Figure **9** reveals that increasing the static load ratio (λ from 0.2 to 0.8) leads to reductions in both the modified natural frequency Ω and the damping coefficient β, while simultaneously amplifying instability through the rapid increase of μ. Specifically, for ϵ = 0.3, μ rises from 0.13 at λ = 0.2 to 0.3 at λ = 0.8, which results in a pronounced exponential escalation of the MLEs as the static load increases.

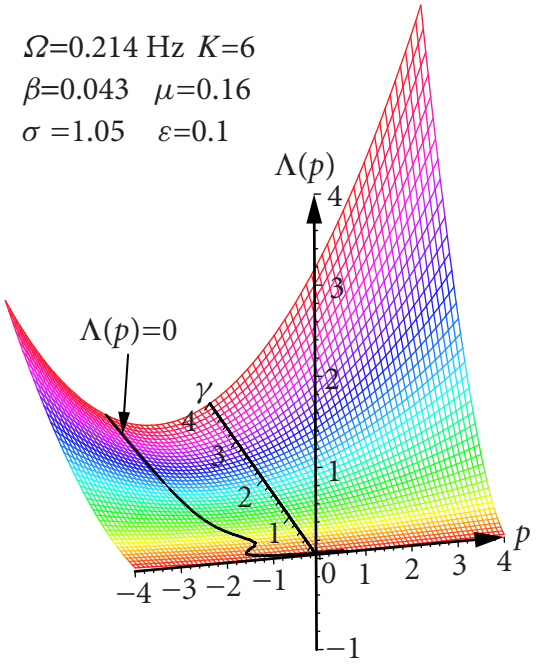

Figure 6: Three-dimensional MLE for amplitude of noise γ.

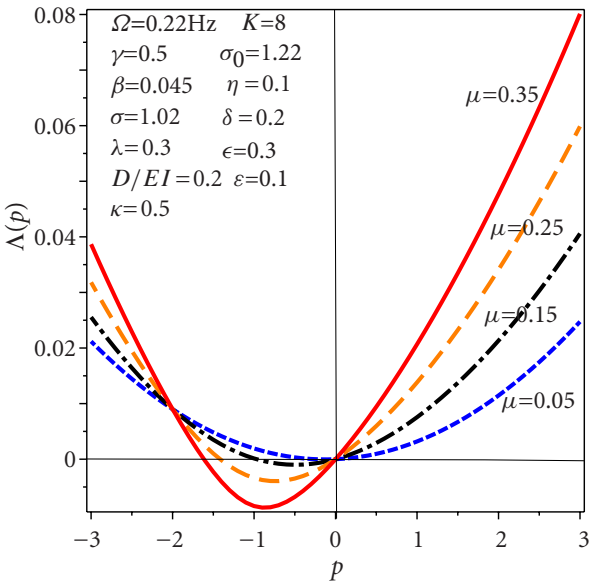

Figure 7: Impact of harmonic amplitude μ on MLEs.

5.3. Effect of soil's damping, stiffness, and flexural rigidity

Figure **10** depicts the instability diagrams corresponding to various levels of foundation damping,

characterized by logarithmic decrements δ = 0.2, 0.4, 0.6, and 0.8 in Equation (**18**). The results indicate that higher damping leads to enhanced stability, as evidenced by the reduction in MLE values. These exponents are computed as nontrivial solutions of Equation (**51**) through an eighth-order Fourier series approximation (K = 8).

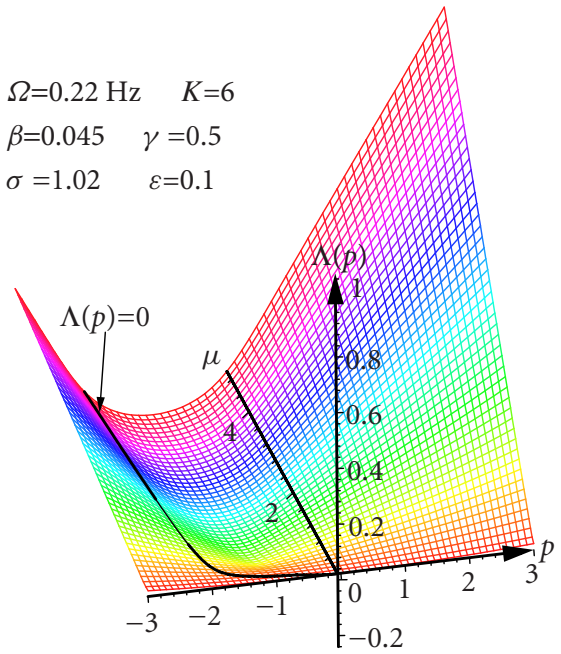

Figure 8: Three-dimensional MLE for harmonic amplitude μ.

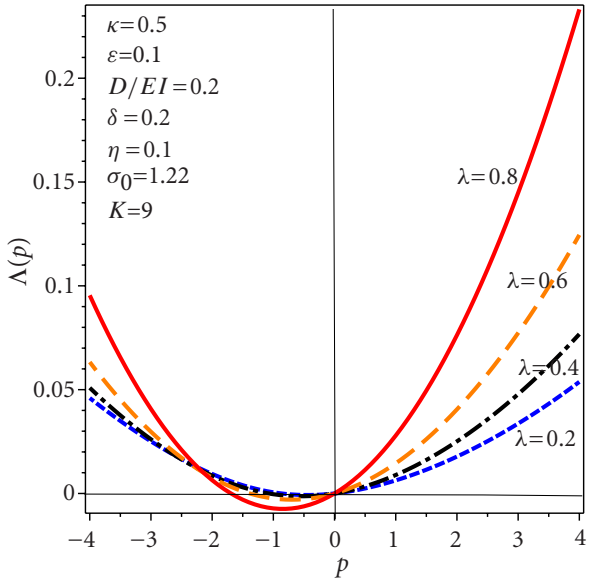

Figure 9: Influence of static loads λ on MLEs.

Figure **11** examines how variations in the soil stiffness parameter η affect the instability characteristics of the system as quantified by the MLEs. An increase in soil rigidity leads to a consistent reduction in MLE values and a corresponding contraction of the instability domains, indicating enhanced system stability. This behavior is attributed to the contribution of a stiffer foundation, which effectively increases the overall damping and alters the modified natural frequency of the pile under combined loading conditions. In a similar context, Figure **12** explores the role of the dimensionless bending parameter $\frac{D}{EI}$ in governing stochastic stability. As $\frac{D}{EI}$ increases, both the effective damping and the modified natural frequency of the pile system rise, resulting in a shift of the modified natural frequency from 0.16 Hz to 0.23 Hz and an increase in the damping coefficient from 0.032 to 0.047 as $\frac{D}{EI}$ varies from 0 to 0.7. Notably, the case $\frac{D}{EI} = 0$ corresponds to the conventional Winkler foundation model.

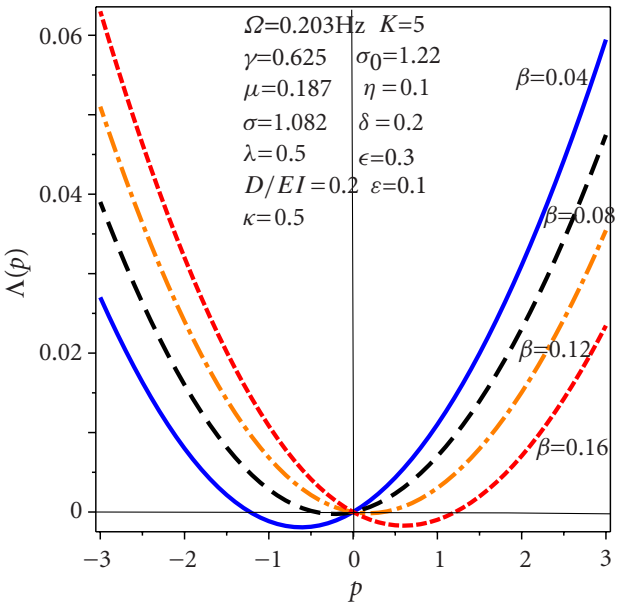

Figure 10: Effect of damping β on MLEs.

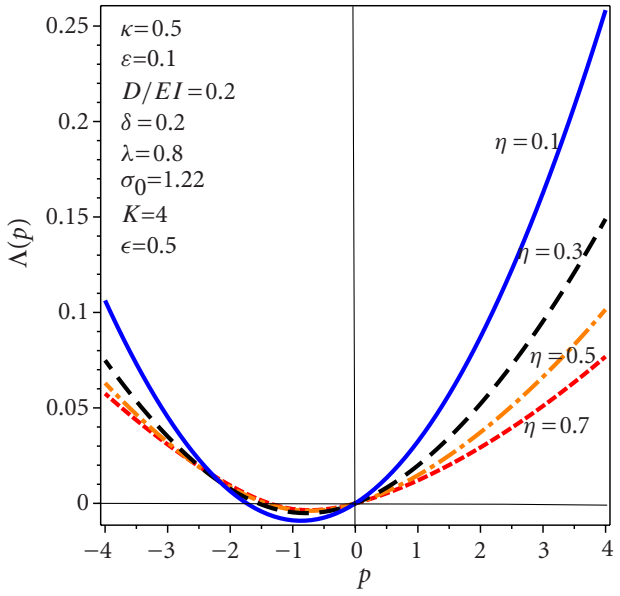

Figure 11: Effect of soil stiffness η on MLEs.

5.4. Effect of pile's geometric and mechanical parameters

Figure (**13** to **15**) provide a systematic assessment of how geometric and mechanical variations of the pile influence both influence both the qualitative response

and quantitative stability metrics of the system. An increase in pile length (Figure **13**) leads to a pronounced reduction in dynamic stability, primarily due to the heightened propensity for higher-mode buckling. In contrast, enlarging the cross-sectional diameter (Figure **14**) and increasing the Young's modulus (Figure **15**) result in clear improvements in stability behavior. These effects are associated with an elevation in the effective natural frequency of the pile–soil system, along with enhanced damping characteristics, both of which act to suppress the activation of higher-order buckling modes under combined static, harmonic, and stochastic loading conditions.

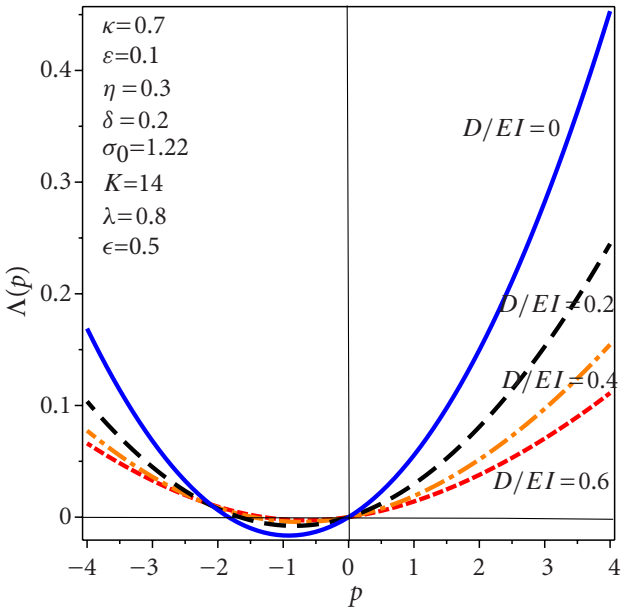

Figure 12: Effect of flexural rigidity $\frac{D}{EI}$ on MLEs.

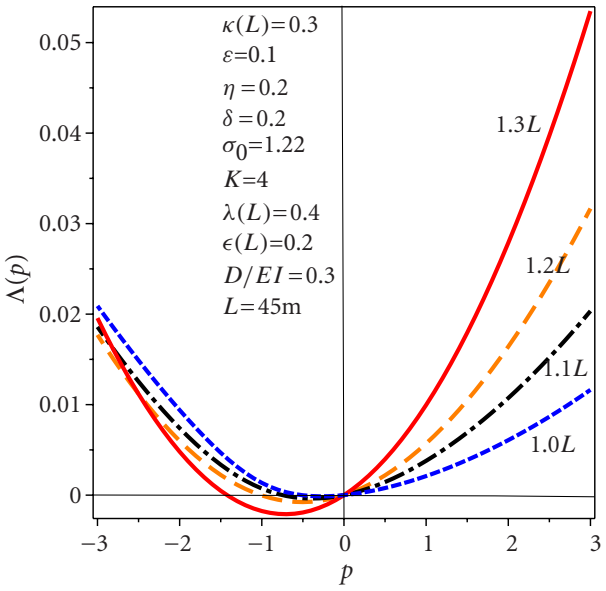

Figure 13: Effect of length L on MLEs.

The parameters $\kappa(\cdot)$, $\lambda(\cdot)$, and $\epsilon(\cdot)$ associated with L, D, and E are defined based on their reference (baseline) configuration corresponding to the unity ratio (i.e., L, D, or E). For scaled cases such as $1.2L$, $1.4D$, or $1.6E$, these parameters are not held constant; instead, they are recalculated consistently according to the updated geometric or material properties, ensuring that κ, λ, and ϵ reflect the modified system characteristics relative to the baseline values.

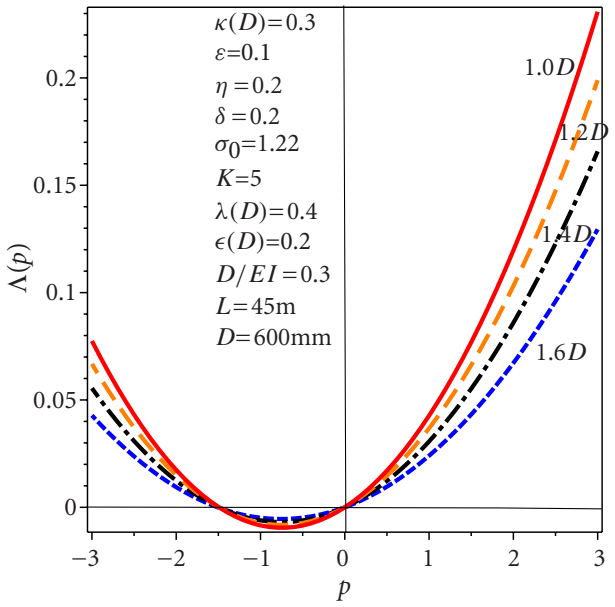

Figure 14: Effect of exterior diameter D on MLEs.

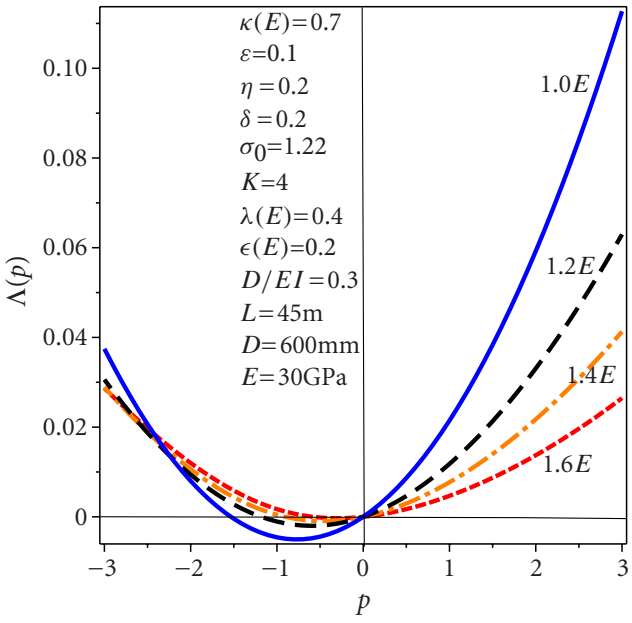

Figure 15: Effect of Young's elastic modulus E on MLEs.

The MLE serves as a quantitative indicator of stability under combined deterministic and stochastic loading. A positive MLE corresponds to exponential growth of response moments, which can be interpreted as a probabilistic form of instability or dynamic buckling. The results demonstrate that increasing soil stiffness and damping significantly enhances stability, suggesting that ground improvement techniques can be effective in mitigating instability risks. Conversely, high stochastic excitation intensity can induce

instability even when deterministic loading conditions are within safe limits, highlighting the importance of incorporating stochastic effects into design frameworks.

Additionally, the findings indicate that longer piles are more susceptible to instability, while increases in material stiffness and cross-sectional dimensions improve stability. These observations provide direct guidance for design optimization and reliability-based assessment of pile foundations subjected to multi-hazard loading conditions.

Previous studies in pile foundation dynamic design have predominantly focused on deterministic loading conditions, where static and harmonic excitations are considered as the primary sources of instability. However, such assumptions do not fully reflect real-world conditions, particularly in the context of seismic loading, which inherently exhibits aperiodic and random characteristics. In reality, earthquake-induced loads cannot be adequately represented by purely deterministic functions due to their stochastic nature and broadband frequency content.

In contrast, the present study advances the existing body of knowledge by incorporating multiple parametric excitations that include not only static and harmonic components but also stochastic Gaussian noise. This formulation provides a more realistic representation of environmental and seismic excitations acting on pile foundations. To the best of the authors' knowledge, the combined effect of deterministic and stochastic parametric excitations on the moment stability of pile systems, analyzed through moment Lyapunov exponents within a unified analytical framework, has not been previously reported. This constitutes a significant extension beyond classical deterministic stability analyses and enables a probabilistic characterization of instability mechanisms that cannot be captured using conventional approaches.

Furthermore, the inclusion of stochastic excitation reveals instability regions that may not be predicted under deterministic assumptions, highlighting the critical role of randomness in dynamic stability assessment. This demonstrates that designs based solely on deterministic models may underestimate instability risks, thereby emphasizing the necessity of stochastic formulations in advanced geotechnical and structural reliability analysis.

6. CONCLUSIONS

This study investigated the dynamic stability of a pile foundation system subjected to multiple parametric stochastic excitations. The governing equation of motion was first formulated and subsequently reduced using Galerkin truncation, resulting in a system of linear stochastic differential equations, which was further decoupled into Itô equations through stochastic averaging. While classical Lyapunov exponents describe almost-sure stability, they do not fully capture moment stability; therefore, MLEs were employed to provide a more comprehensive stability assessment. An efficient analytical framework was established by transforming the decoupled Itô system into an eigenvalue problem, enabling the derivation of MLEs via Fourier series expansion and the determination of stability boundaries and indices. To obtain MLEs numerically and to validate the analytical findings and evaluate the applicability of the stochastic averaging approach, Monte Carlo simulations were conducted using a Taylor-based discretization scheme. The close agreement between analytical predictions and numerical results confirms the accuracy and robustness of the proposed methodology.

The results indicate that high noise intensity significantly amplifies parametric resonance, while increases in both the harmonic excitation amplitude μ and the stochastic excitation amplitude further contribute to system destabilization. In contrast, damping plays a stabilizing role by reducing the magnitude of the MLEs and enlarging the stability regions. Improvements in soil stiffness and flexural rigidity enhance stability by increasing effective damping and altering the system's natural frequency, thereby suppressing higher-order buckling modes. On the other hand, increasing the pile length reduces dynamic stability, whereas higher Young's modulus and larger cross-sectional diameter improve structural rigidity and counteract destabilizing effects under combined loading conditions. Additionally, the static load ratio is identified as key contributor to instability mechanisms within the system.

The present study is based on several simplifying assumptions that define its range of applicability. The stochastic averaging method assumes weak excitation and small damping, and its accuracy may deteriorate under strong stochastic forcing. In addition, the soil–structure interaction is modeled using a linear elastic foundation, which does not capture nonlinear effects such as soil yielding, separation, or cyclic degradation. Furthermore, the SDOF approximation neglects higher-mode interactions that may become significant in complex loading scenarios. Future work should address these limitations by extending the framework to nonlinear foundations, multi-mode systems, and colored noise excitation models.

Credit Authorship Contribution Statement

Vahdat Samandar Ajirlou: Writing – original draft, Investigation, Software, Resources, Data curation.

Jian Deng: Writing – review & editing, Supervision, Visualization, Validation, Project administration, Funding acquisition, Conceptualization.

DECLARATION OF COMPETING INTEREST

The authors declare that they have no known competing financial interests or personal relationships that could have appeared to influence the work reported in this paper.

ACKNOWLEDGMENTS

The authors acknowledged the support from Natural Sciences and Engineering Research Council of Canada (NSERC) through discovery grants (RGPIN-2025-07106).

NOTATIONS

E	Young's elastic modulus
I	moment of inertia
ρ	mass density
k_s	Winkler foundation's stiffness coefficient per unit length
c_s	damping coefficient per unit length
x	pile's longitudinal axis
δ	foundation damping's logarithmic decay measurement
P_s	constant longitudinal compressive force
Ω_0	modified natural frequency of system
ω_0	natural frequency of system
P_E	Euler buckling load
λ	non-dimensional static load
ϵ	non-dimensional dynamic force
κ	dimensionless stochastic load
η	foundation stiffness
μ_0	coefficient of the harmonic load
γ_0	coefficient of the stochastic load
$W(\tau)$	standard Wiener process
Δt	time step size
σ_0	diffusion coefficient
$\mathbf{X}(\tau)$	state vector
$\Lambda(p)$	moment Lyapunov exponent
$\mathcal{R}(\tau)$	autocorrelation function of stochastic noise $\xi(t)$
$\mathcal{T}(\varphi)$	eigenfunction
$\mathbb{S}$	independent sample paths
$\mathbf{x}^s(t_\varkappa)$	sth sample of the vector of the response variables at time t_k
$\|\mathbf{x}^s(t_\varkappa)\|$	Euclidean norm
L	length of pile
A	cross-sectional area of pile

REFERENCES

[1] Prakash, S., Sharma, H.D. (1991). Pile Foundations in Engineering Practice. John Wiley & Sons.

[2] Bhattacharya, S., Goda, K. (2013). Probabilistic buckling analysis of axially loaded piles in liquefiable soils. Soil Dynamics and Earthquake Engineering, 45: 13-24.

[3] Zhang, X., Tang, L., Ling, X., Chan, A. (2020a). Critical buckling load of pile in liquefied soil. Soil Dynamics and Earthquake Engineering, 135: 106197.

[4] Zhang, X., Tang, L., Ling, X., Chan, A. (2020b). Effect of the combined action of lateral load and axial load on the pile instability in liquefiable soils. Engineering Structures, 205: 110074.

[5] Ajirlou, V.S., Ranjbarnia, M., Oreste, P. (2023). Theoretical modeling of the pre-cutting system performance for the tunnel face stability in very weak rock masses. Transportation Geotechnics, 42: 101073.

[6] Ajirlou, V.S., Ranjbarnia, M., Dias, D. and Deng, J. (2025). Pre-support shell system for the face stability of deep tunnels in weak grounds: using theory of cylindrical shell. Structures, 71:108180.

[7] Madabhushi, G., Haigh, S., Knappett, J. (2009). Design of Pile Foundations in Liquefiable Soils. World Scientific.

[8] Stratonovich, R.L. (1967). Topics in the Theory of Random Noise. CRC Press.

[9] Khasminskii, R.Z. (1966). A limit theorem for the solutions of differential equations with random right-hand sides. Theory of Probability & Its Applications, 11(3): 390-406.

[10] Xie, W-C. (2006). Dynamic Stability of Structures. Cambridge University Press.

[11] Roberts, J.B., Spanos, P.D. (1986). Stochastic averaging: an approximate method of solving random vibration problems. International Journal of Non-linear Mechanics, 21(2): 111-34.

[12] Ariaratnam, S. T. (1995). Stochastic stability of viscoelastic systems under bounded noise excitation. In: IUTAM Symposium on Advances in Nonlinear Stochastic Mechanics: Proceedings of the IUTAM Symposium, Trondheim, Norway: 11-18.

[13] Sri Namachchivaya, N.S., Ariaratnam, S.T. (1987). Periodically perturbed Hopf bifurcation. SIAM Journal on Applied Mathematics, 47(1): 15-39.

[14] Ariaratnam, S.T. (1993). Stochastic stability of linear viscoelastic systems. Probabilistic Engineering Mechanics, 8(3-4): 153-5.

[15] Ariaratnam, S.T., Tam, D.S.F., Xie, W-C. (1991). Lyapunov exponents and stochastic stability of coupled linear systems under white noise excitation. Probabilistic Engineering Mechanics, 6(2): 51-6.

[16] Hu, D., Guo, N., Zhao, K., Guirao, J.L.G, Chen, H. (2024). Moment Lyapunov exponent and stochastic stability of a vibro-impact system driven by non-Gaussian colored noise. International Journal of Non-linear Mechanics, 161: 104693.

[17] Deng, J., Xie, W-C., Pandey, M.D. (2014a). Higher-order stochastic averaging to study stability of a fractional viscoelastic column. Journal of Sound and Vibration, 333(23): 6121-39.

[18] Deng, J., Xie, W-C., Pandey, M.D. (2014b). Stochastic stability of a fractional viscoelastic column under bounded noise excitation. Journal of Sound and Vibration, 333(6): 1629-43.

[19] Deng, J. (2018). Stochastic stability of coupled viscoelastic systems excited by real noise. Mathematical Problems in Engineering, (1): 4725148.

[20] Sri Namachchivaya, N., Van Roessel, H.J. (2001). Moment Lyapunov exponent and stochastic stability of two coupled oscillators driven by real noise. Journal of Applied Mechanics, 68(6): 903-14.

[21] Stojanović, V., Deng, J., Petković, M.D., Milić, D. (2025). Modeling of Complex Dynamic Systems: Fundamentals and Applications. Elsevier.

[22] Engel, R.S. (1991). Dynamic stability of an axially loaded beam on an elastic foundation with damping. Journal of Sound and Vibration, 146(3): 463-77.

[23] Deng, J., Shahroudi, M., Liu, K. (2023). Dynamic stability and responses of beams on elastic foundations under a parametric load. International Journal of Structural Stability and Dynamics, 23(02): 2350018.

[24] Rao, S.S. (2019). Vibration of Continuous Systems. John Wiley & Sons.

[25] Cai, G.Q., Zhu, W.Q. (2016). Elements of Stochastic Dynamics. World Scientific Publishing.

[26] Bolotin, V.V. (1964). The Dynamic Stability of Elastic Systems. Holden-Day Inc., San Francisco.

[27] Xu, X., Zhang, Z., Yao, W., Zhao, Z. (2021). Dynamic stability analysis of pile foundation under wave load. International Journal of Geomechanics, 21(4): 04021021.

https://doi.org/10.65904/3083-3590.2026.02.02

© 2026 Ajirlou and Deng.
This is an open access article licensed under the terms of the Creative Commons Attribution License (http://creativecommons.org/licenses/by/4.0/) which permits unrestricted use, distribution and reproduction in any medium, provided the work is properly cited.